Multiprobe molecular imaging of an NMDA receptor hypofunction rat model for glutamatergic dysfunction

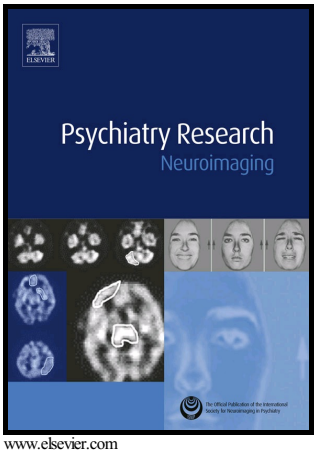

Multiprobe molecular imaging of an NMDA receptor hypofunction rat model for glutamatergic dysfunction

Lauren Kosten, Jeroen Verhaeghe, Robert Verkerk, David Thomae, Livia De Picker, Leonie wyffels, Annemie Van Eetveldt, Stefanie Dedeurwaerdere, Sigrid Stroobants, Steven Staelens

PII: S0925-4927(16)30017-8
DOI: http://dx.doi.org/10.1016/j.pscychresns.2016.01.013
Reference: PSYN10501

To appear in: *Psychiatry Research: Neuroimaging*

Received date: 16 June 2015
Revised date: 23 December 2015
Accepted date: 7 January 2016

Cite this article as: Lauren Kosten, Jeroen Verhaeghe, Robert Verkerk, David Thomae, Livia De Picker, Leonie wyffels, Annemie Van Eetveldt, Stefanie Dedeurwaerdere, Sigrid Stroobants and Steven Staelens, Multiprobe molecular imaging of an NMDA receptor hypofunction rat model for glutamatergic dysfunction, *Psychiatry Research: Neuroimaging* http://dx.doi.org/10.1016/j.pscychresns.2016.01.013

MULTIPROBE MOLECULAR IMAGING OF AN NMDA RECEPTOR HYPOFUNCTION RAT MODEL FOR GLUTAMATERGIC DYSFUNCTION

Lauren Kostena, Jeroen Verhaeghea, Robert Verkerkb, David Thomaea,d, Livia De Pickerc,
Leonie wyffelsa,d, Annemie Van Eetveldte, Stefanie Dedeurwaerderee, Sigrid Stroobantsa,d, Steven Staelensa*

a. Molecular Imaging Center Antwerp, University of Antwerp, Antwerp, Belgium.
b. Laboratory of Medical Biochemistry, Department of Pharmaceutical Sciences, University of Antwerp, Antwerp, Belgium.
c. Collaborative Antwerp Psychiatric Research Institute, University of Antwerp, Antwerp, Belgium.
d. Department of Nuclear Medicine, University Hospital Antwerp, Antwerp, Belgium.
e. Translational Neurosciences, University of Antwerp, Antwerp, Belgium.

*Corresponding author. Tel: +32 (0)3 265 2820; fax: +32 (0)3 265 2813.

steven.staelens@uantwerpen.be

Abstract

There are many indications of a connection between abnormal glutamate transmission through N-methyl-D-aspartate (NMDA) receptor hypofunction and the occurrence of schizophrenia. The importance of metabotropic glutamate receptor subtype 5 (mGluR5) became generally recognized due to its physical link through anchor proteins with NMDAR. Neuroinflammation as well as the kynurenine (tryptophan catabolite; TRYCAT) pathway are equally considered as major contributors to the pathology.

We aimed to investigate this interplay between glutamate release, neuronal activation and inflammatory markers, by using small-animal positron emission tomography (PET) in a rat model known to induce schizophrenia-like symptoms.

Daily intraperitoneal injection of MK801 or saline were administered to induce the model together with N-Acetyl-cysteine (NAc) or saline as the treatment in 24 male Sprague Dawley rats for one month. Biweekly *in vivo* [^{11}C]-ABP688 microPET was performed together with mGluR5 immunohistochemistry. Simultaneously, weekly *in vivo* [^{18}F]-FDG microPET imaging data for glucose metabolism was acquired and microglial activation was investigated with

biweekly *in vivo* [^{18}F]-PBR111 scans versus OX42 immunohistochemistry. Finally, plasma samples were analyzed for TRYCAT metabolites.

We show that chronic MK801 administration (and thus elevated endogenous glutamate) causes significant tissue loss in rat brain, enhances neuroinflammatory pathways and may upregulate mGluR5 expression.

Key words: schizophrenia; glutamate; molecular imaging; animal model; TRYCAT

Abbreviations

BPnd: Non-displacable binding potential; *CG*: Cingulate cortex; *CP*: Caudate putamen; *CT*: Computed tomography; *Ctrl*: Control; *Ctrl-PBO*: Placebo-treated control cohort; *Ctrl-NAc*: NAc-treated control cohort; *FOV*: Field of view; *GSH*: Glutathion; *HC*: Hippocampus; *HPLC*: High-pressure liquid chromatography; *IDO*: Indoleamine-2,3-deoxygenase; *IHC*: Immunohistochemistry; *IOD*: Intrinsic optical density; *i.p.*: intraperitoneal; *i.v.*: intravenous; *KA*: Kynurenic acid; *KAT*: Kynurenine amino transferase; *KYN*: Kynurenine; *mGluR*: Metabotropic glutamate receptor; *mPFC*: Medial prefrontal cortex; *NAc*: N-Acetyl-cysteine; *NMDA*: N-methyl-D-aspartate; *PBO*: Placebo; *PET*: Positron emission tomography; *p.i.*: post injection; *QA*: Quinolinic acid; *ROI*: Region of interest; *SUV*: Standard uptake value; *MK-PBO*: Placebo-treated schizophrenia-like cohort; *MK-NAc*: NAc-treated schizophrenia–like cohort; *TDO*: Tryptophan-2,3-deoxygenase; *TRYCAT*: Tryptophan catabolite; *TSPO*: Translocator protein; *VOI*: Volume of interest; *3-HK*: 3-hydroxykynurenine; *%ID*: percentage injected dose

1. Introduction

Schizophrenia is a psychiatric disorder affecting about 0.7-1% of the world's population (Preti and Wilson, 2011) and represents an important cause of chronic invalidity. The term schizophrenia is applied to a syndrome characterised by long disease duration, positive symptoms (e.g. delusions and hallucinations that occur in psychotic episodes), negative symptoms (e.g. social withdrawal and anhedonia) and cognitive symptoms (i.e. difficulty with abstract thinking and executive functioning) (van Os and Kapur, 2009). Much about the etiology and pathophysiology of schizophrenia remains unknown. The main hypothesis involves the dopaminergic system, however more recently there are many additional indications for a connection between N-methyl-D-aspartate (NMDA) receptor hypofunction and glutamate imbalances with the manifestation of schizophrenia (Vinson and Conn, 2012). The proposed mechanism of the NMDAR hypofunction theory in schizophrenia is illustrated in figure 1A. The reduced function of this NMDA receptor is already demonstrated in schizophrenia subjects (Nakazawa et al., 2012). In addition, multiple aspects mimicking the human brain pathophysiology can be induced in animal models by administration of NMDAR-antagonists (Bubeníková-Valešová et al., 2008) such as dizocilpine (MK801; figure 1A(3)-B). These animal models provide a useful instrument to unravel the mechanisms of schizophrenia, and to screen for new promising therapies. The abnormal glutamate neurotransmission observed in schizophrenia (Gaspar et al., 2009), is also implicated in the pathophysiology of various other neuropsychiatric disorders (Fatemi and Folsom, 2015).

Imaging studies revealed reduced NMDAR binding in patients with schizophrenia, yet targeting this receptor is not considered a viable option due to potential overactivation and neurotoxicity. Therefore there have been attempts to target the metabotropic receptors which function to modulate synaptic transmission (Matosin and Newell, 2013; Vinson and Conn, 2012). Glutamatergic proteins are expressed at neuronal membranes as well as on microglia and astrocytes (Zantomio et al., 2015). Metabotropic glutamate receptor subtype

5 (mGluR5) is of importance in the communication between neurons and glial cells, including control of glutamate release and uptake by astrocytes. The importance became generally recognized due to its physical link through anchor proteins with NMDAR and since the discovery of the therapeutic effects of mGluR5 positive allosteric modulators (Hashimoto et al., 2013). Thus far literature suggests contradictive results, such as no alterations in total mGluR5 expression in the schizophrenia post-mortem brain (Newell and Matosin, 2014), reduced mGluR5 protein levels and mRNA levels (Fatemi and Folsom, 2015; Fatemi et al., 2013) or increased expression (Meador-Woodruff, 2000).

Coupled with the glutamatergic hypothesis for the etiology of schizophrenia, interest has grown for neuroinflammation and associated neurodegeneration as a major pathophysiological contributor. Increased global and focal activation of microglia was found in brains from schizophrenia subjects both postmortem and *in vivo* with TSPO PET scan (Bayer et al., 1999; van Berckel et al., 2008). Inflammation also potentially influences glutamatergic systems through microglial glutamate release as an indirect consequence of decreased glutathione (GSH) levels (Barger et al., 2007) (figure 1A(3)). This mechanism has been shown in schizophrenia patients and can be induced by administration of exogenous NMDAR antagonists (Radonjić et al., 2010). Activated microglia stimulate astrocytes and these astrocytes respond by releasing excessive glutamate that binds to mGluR5 receptors on neurons and induces neuroinflammation through neurotoxicity (Zantomio et al., 2015).

N-Acetyl-cysteine (NAc) shows beneficial effects in schizophrenia-like pathology and it has previously been postulated that the main benefits would be through restoration of depleted GSH levels - which normalizes microglial glutamate release and stimulates the NMDAR input to inhibitory GABA-ergic interneurons through its redox modulatory site, as illustrated in figure 1A(11) - and direct scavenging of free radicals (Berk et al., 2013; Dean et al., 2012). Additionally, NAc activates the cysteine-glutamate antiporter, thereby increasing the

extrasynaptic glutamate release, hence reducing the glutamate release in the synaptic cleft through stimulation of its reuptake via mGluR2/3. Thus, NAc can counteract the glutamate release induced by the microglial response. NAc is also known to block the expression of CD11b on microglia. It therefore has an anti-inflammatory effect by tempering the severity of microglial activation which dampens inflammation and neuronal degeneration. (Wang et al., 2009) and is therefore selected as the treatment paradigm in this study.

We aimed to investigate this interplay between glutamate release, neuronal activation and inflammatory markers, by performing an *in vivo* longitudinal multiprobe microPET/CT study in a rat model of NMDA receptor hypofunction, a well described model for schizophrenia (Eyjolfsson et al., 2006; Huang et al., 2012). As aforementioned, endogenous glutamate levels were increased through a pharmacological challenge with MK801, an NMDA receptor antagonist, as in figure 1A-B. Firstly, both in NMDAR antagonism (figure 1A) and schizophrenia patients (Park et al., 2006; Soyka et al., 2005; Whitfield-Gabrieli et al., 2009) altered neuronal metabolism has been demonstrated. Here, neuronal metabolism was imaged using [^{18}F]-fluorodeoxyglucose ([^{18}F]-FDG) microPET/CT, as in figure 1A(4). Secondly, microglial activation was investigated with [^{18}F]-PBR111, a radiotracer that binds to translocator protein (TSPO) receptors which are upregulated in activated microglia as shown in figure 1A(8), making [^{18}F]-PBR111 a suitable biomarker for microglial activation, indicating neuroinflammation (Fookes et al., 2008). Thirdly, [^{11}C]-ABP688 [3-(6-methyl-pyridin-2-ylethynyl)-cyclohex-2-enone-O-11C-methyloxime], a highly selective allosteric antagonist of the metabotropic glutamate 5 receptor (mGluR5 figure 1C) (Elmenhorst et al., 2012), was used to image and measure hypothesized mGluR5 alterations (figure 1A(1)) (Deschwanden et al., 2011; Miyake et al., 2011; Poels et al., 2014; Sandiego et al., 2013; Wyckhuys et al., 2013).

Additionally, as a complement we studied the role of the TRYCAT pathway, a major catabolic

cascade of tryptophan (TRP) as illustrated in figure 1D. In the CNS, the TRYCAT pathway takes predominantly place in microglia and astrocytes, and is upregulated in neuroinflammatory conditions (Chen and Guillemin, 2009). The ratio between metabolite (kynurenines) concentrations gives an indication of changes in enzyme activity and therefore pathway direction. The rate-limiting step is the conversion of TRP to kynurenine (KYN). The TRYCAT pathway splits up in a neurodegenerative arm and a neuroprotective arm leading to the generation of quinolinic acid (QA) and kynurenic acid (KA), respectively. The generation of neurotoxins, like the excitotoxic NMDAR-agonist QA, or apoptogenic 3-hydroxykynurenine (3-HK), through the indoleamine 2,3-dioxygenase (IDO)-initiated branch of the TRYCAT pathway provide further support for the neuronal degeneration hypothesis. On the other hand the neuroprotective metabolite NMDAR-antagonist KA, formed in the tryptophan 2,3- dioxygenase (TDO)-initiated branch of the pathway, can counteract the effect of QA on NMDAR when the different metabolites are well balanced (Myint, 2012). Microglial activation should be regarded as a part of systemic activation of immuno-inflammatory pathways, with inflammation and alterations in kynurenines. A hyperactive pro-inflammatory response will upregulate TRYCAT pathway in activated microglia (Anderson et al., 2013) through IDO, contributing again to increased glutamate as in figure 1A(5) (Anderson and Maes, 2013). If microglial activation contributes to the pathophysiology of schizophrenia, then direct modulators of microglia function may be effective in the treatment of psychotic disease. (Frick et al., 2013)

In individuals with schizophrenia, imbalance between the metabolites QA and KA has been found, possibly contributing to the pathology (Myint, 2012). Therefore, we analyzed plasma samples for kynurenines with high-pressure liquid chromatography (HPLC).

2. Materials and methods

2.1. Radiosynthesis

[^{18}F]-FDG and [^{11}C]-ABP688 were prepared as previously published (Wyckhuys et al., 2013; 2014). A detailed description of the radiosynthesis of [^{18}F]-PBR111 is provided in the supplemental data. [^{18}F]-FDG is a glucose analog with the ^{18}F isotope substituted for the normal hydroxyl group at the 2' position in the glucose molecule and tissue uptake is a marker for glucose consumption. [^{11}C]-ABP688 is a non-competitive and highly selective antagonist for mGluR5. [^{18}F]-PBR111 is a TSPO ligand which allows PET imaging of cellular activation during neuroinflammation. TSPO is a mitochondrial membrane protein with a low level of expression in resident glial cells of the healthy brain, while its expression is dramatically enhanced after activation of glial cells.

2.2. Animals

Twenty-four male Sprague Dawley rats (age 7 weeks; 289.67 ±10.37g at baseline; Janvier Laboratories, Le Genest-St-Isle, France) received two daily intraperitoneal (i.p.) injections during four weeks. The first injection was either a challenge dose of 0.3 mg/kg (Huang et al., 2012) of the NDMAR antagonist MK801 for the diseased groups (MK) or a comparable volume of saline for the control animals (Ctrl). The second injection, following 30 minutes after the first injection, was either 65 mg/kg N-acetyl-cysteine (NAc) for the treatment groups or saline as placebo (PBO). Injections were given in the evening, while scans were carried out during the day to eliminate acute effects after injection. The total group (n=24) was subdivided in a Ctrl cohort (n=8) and two MK cohorts (both n=8). The Ctrl cohort and one MK cohort both underwent [^{18}F]-FDG PET/CT every week for a month and [^{11}C]-ABP688 PET/CT scans at 0, 2 and 4 weeks. A separate (satellite) MK cohort (n=8) was added to decrease the total scanning burden and these animals underwent [^{18}F]-PBR111 PET/CT at 0, 2 and 4 weeks. In each cohort half of the animals were NAc-treated (n=4), while the other

received the PBO injection (n=4) as summarized in figure 2A. The study protocol was approved by the local Animal Experimental Ethical Committee of the University of Antwerp, Belgium (ECD 2013-13). All scans and catheter insertions were performed under isoflurane anesthesia and all efforts were made to minimize animal suffering.

2.3. PET-acquisitions

For optimal throughput animals were positioned head-to-head in the field-of-view (FOV) on a Siemens Inveon PET-CT scanner (Siemens Preclinical Solution, Knoxville, TN, USA).

Static acquisitions were performed for both [^{18}F]-FDG and [^{18}F]-PBR111 scans, as illustrated in figure 2B and 2C respectively. Briefly, animals were shortly anesthetized with 1.5% isoflurane gas anesthesia prior to i.v. injection with the tracer in the tail vein (Supplemental data table 1), followed by an uptake period before scanning. Each scan was followed by a 10-min 70 kV/500 µA CT scan for co-registration with PET data. For [^{18}F]-FDG acquisitions, animals were fasted overnight for at least 12 hours (Deleye et al., 2014) and blood glucose measurements were taken at the time of tracer injection for correction of the microPET data with blood glucose levels.

For [^{11}C]-ABP688 scans, dynamic acquisitions were performed as illustrated in figure 2D through simultaneous tracer injection and start of the scan. The injected tracer volume was 0.5 mL. Image processing is described in detail in the supplemental methods.

2.4. Kynurenines

Blood samples were collected from the tail vein at baseline, after two weeks and after 4 weeks, as shown in figure 2A. Samples were taken in EDTA-coated tubes and centrifuged (1057g; 10 min; 4°C) to collect plasma. Plasma samples were stored at -80°C until further analysis.

Metabolites from the TRYCAT pathway (figure 1D), more specifically tryptophan (TRP), kynurenine (KYN), kynurenic acid (KA) and quinolinic acid (QA) levels were analysed using high-pressure liquid chromatography (HPLC; Chromolith Performance 2.0 x 100 mm with Chromolith guard cartridge). Methods of analysis are described in detail in the supplemental methods.

2.5. Immunohistochemistry

Immunohistochemical staining techniques and corresponding fixation are summarized in figure 2A (and described in detail in the supplemental methods). In short, immediately after the rats received their last scan, they were given an overdose of sodium pentobarbital (150mg/kg), followed by decapitation. Brains were dissected and snap frozen in liquid nitrogen. All samples were stored at -80°C until further analysis. Staining was performed using cresyl violet, mGluR5 and OX42. All pictures were taken with an Olympus CX31RBSF microscope, digitalised by Nikon Digital Sight DS-U3 and DS-Fi1 camera, using NIS elements software version 4.2. (Nikon Instruments). Neuronal damage was assessed on cresyl violet staining. Using Image J cell counting software (Image J version 1.47), the number of neurons and the number of damaged neurons was counted in at least five different 40x images per brain region, followed by calculation of percentage damage. OX42 DAB staining intensity was scored based upon the number of stained cells, intensity of the staining and morphology, as described in literature (Van den Eynde et al., 2014). The score is calculated in at least five different 40x images per brain region of the most densely stained areas. The mGluR5 receptor immunoreactivity was semi-quantitatively measured. Integrated optical density was calculated using NIS elements software version 4.2 at 40x magnification, in 5 images taken in the brain structure regions of interest (ROI). Results for the multiple images were then averaged per ROI.

The PET and IHC data were analyzed in four clearly identifiable and relevant brain areas: (1)

The caudate putamen (CP), as during psychosis, coherent intrinsic activity of the dorsal striatum increases and correlates with positive symptoms such as delusion and hallucination (Sorg et al., 2013). (2) The cingulate cortex (CG), as the pathology in the anterior cingulate cortex is widely believed to have a significant role in the disease process of schizophrenia. The cingulate cortex receives inputs from the thalamus and is an integral part of the limbic system, which makes it highly important in cognitive function (Adams and David, 2007). (3) The medial prefrontal cortex (mPFC), which is also involved in negative symptoms due to hypofrontality, and (4) the hippocampus (HC), as an increased hippocampal drive to the ventral tegmental area is involved in striatal hyperdopaminergia (Adams et al., 2013).

2.6. Statistical analyses

Due to a high number of groups and hence a rather limited group size, statistical assumptions needed for parametrical testing could not be made and non-parametric tests were applied. For longitudinal testing, the Dunnett's multiple comparison was used as it takes into consideration the special structure of comparing treatment against control i.e baseline and results in narrower confidence intervals with the total sample size minus the number of groups as degrees of freedom. When main effects were found for a time point, further analyses were carried out for each condition. Kruskal-Wallis tests determined differences between condition with the degrees of freedom at each instance being the number of groups minus 1. When significant, Mann-Whitney U tests were used for pairwise comparison with each group's size as degrees of freedom. Spearman correlations determined correlations between histological data and PET imaging data and between plasma metabolites. Data was considered significant if p-values < 0.05. All data are expressed as mean ± SD, unless otherwise stated.

3. Results

3.1. Brain glucose metabolism

The results of the glucose metabolism, as measured with [^{18}F]-FDG SUV, are shown in figure 3A-D and illustrated in supplemental figure 1. The [^{18}F]-FDG uptake within the MK-PBO cohort was decreased compared to t=0w at all time points, peaking from -20.94%±15.75% (HC; significant over time $p<0.001$) up to -28.42%± 15.46% (mPFC; significant over time $p<0.001$) at t=2w, while in Ctrl-PBO animals SUV increases were detected in part due to weight gain over time, as described by Deleye *et al.* (Deleye et al., 2014) . Differences between the MK-PBO cohort and the Ctrl-PBO cohort are significant already in the first week for all regions ($p<0.05$). This decrease was moderately remedied by NAc, though a significant treatment effect was only noted after 2 weeks. Importantly, supplemental figure 3 shows cresyl violet staining revealing widespread tissue damage in the MK-PBO cohort. From figure 4A it can be seen that this tissue damage is statistically significant for both the CP and HC ($p= 0.021$ and $p=0.043$ respectively). Animals in the MK-NAc cohort show significantly less tissue damage in both structures ($p=0.043$) compared to MK-PBO animals. Spearman correlation analysis revealed a significant negative correlation coefficient of -0.602 ($p=0.014$) for CP, and -0.527 ($p=0.036$) for HC between the percentage of tissue damage and the percentage change to baseline uptake (expressed as %ID) at the final time point.

3.2. Neuroinflammatory markers

Figure 3E-H shows for the satellite MK-PBO cohort decreases in the ratio brain activity/plasma activity (30 min p.i.) for the static [^{18}F]-PBR111 scans at t=2w of -27.6±28% in the caudate putamen (CP; figure 3E; significant over time $p<0.05$) and -19.3±19.4% in the medial prefrontal cortex (mPFC; figure 3F; significant over time $p<0.05$), yet only slight changes of +4.8±10.2% and -4.2±24.2% in the cingulate cortex (CG; figure 3G) and HC (figure 3H). NAc treatment at t=2w results in increases of +33.4±36.2% and +19.5±30.2% for CG and

HC respectively as shown in figure 3G and 3H (not significant over time). At t=4w the [^{18}F]-PBR111 brain/plasma activity ratio was decreased in all animals and all regions compared to t=0w: -61.4±10.4%, -49.4±14%, -37.7±11.6% and -48.5±11% for CP, mPFC , CG and HC respectively in the satellite MK-PBO cohort (all regions significant over time $p<0.001$), and -62±8.5%, -49.3±13.8%, -25.6±10.5% and -35.9±4.9% in the same respective regions in the satellite MK-NAc cohort (in CP, mPFC and HC significant over time $p<0.001$). The treatment effect after 4 weeks was only significant in the HC ($p=0.043$), as shown in figure 3H. In contrast, supplemental figure 4 illustrates OX42 staining, which reveals significantly higher microglial activation in the MK-PBO cohort animals compared to saline control in mPFC, CG, CP and HC ($p\leq0.028$), as shown in figure 4B. Activation in MK-NAc cohort animals was still higher than both Ctrl-NAc and Ctrl-PBO animals in all regions ($p\leq0.018$).

3.3. mGluR5-binding

From figure 3I-L an insignificant increasing BP_{nd} over time can be seen in the MK cohorts. At t=4w BP_{nd} is increased by 9.6%±17.4% compared to t=0w in the mPFC and 9.6%±14.1% for CG, 2.7%±6.1% increased in the CP and 2.4%±10.7% increased in the HC for the MK-PBO cohort. NAc treatment causes a BP_{nd} increase of 16.8±16.2%, 11.8±15.0%, 11.9±17.2% and 19.8±23.3% for the MK-NAc cohort in CG, mPFC, CP and HC respectively at t=4w, not showing significance over time. BP_{nd} PET images are shown in supplemental figure 2. Though not significant, mGluR5 staining in supplemental figure 4 illustrates a tendency to higher intrinsic optical density (IOD) as quantified in figure 4C, in the MK-PBO and MK-NAc cohort compared to Ctrl-PBO in the CG, CP and mPFC. Spearman correlation analysis between IHC and BP_{nd} data from the last scan reveals a significant positive correlation coefficient of 0.625 ($p=0.013$) in CP.

3.4. Kynurenines

The ratio between metabolite concentrations is shown in figure 5A-D. The KYN/TRP ratio is significantly increased after two weeks (p=0.030) in the MK-PBO cohort, with significant differences between Ctrl-PBO and MK-PBO cohort at this time point (p=0.017) and a significant NAc treatment effect is visible in the MK-NAc cohort (p=0.046). Equally, after 2 weeks, the KA/KYN decreased significantly with a model effect between the Ctrl-PBO cohort and MK-PBO cohort (p=0.017), as well as there was a significant treatment effect between MK-PBO and MK-NAc cohorts (p=0.012).

As shown in figure 5C and Figure 5D for t=4w, the Ctrl-NAc cohort significantly differs from the MK-PBO cohort (p=0.007) and Ctrl-PBO cohort (p=0.021) for the QA/KYN as well as for the QA/KA ratio which is also significantly higher for Ctrl-NAc cohort than for the Ctrl-PBO cohort (p=0.029), the MK-PBO (p=0.028) and MK-NAc (p=0.004) cohorts respectively.

4. Discussion

With respect to the glucose metabolism results it should be noted that [^{18}F]-FDG PET measures the phosphorylation of glucose to glucose-6-phosphate and both normal and inflammatory regions take up [^{18}F]-FDG. Consequently, the effects of inflammation should be taken into consideration (Tsukada et al., 2014) when interpreting an increase in [^{18}F]-FDG PET. The [^{18}F]-FDG uptake within the MK-PBO cohort was however decreased compared to t=0w at all time points, while in Ctrl-PBO animals SUV increases were detected in part due to body weight gain. The percentage decrease in [^{18}F]-FDG uptake compared to baseline for the MK-PBO cohort are in accordance with literature about chronic exposure to NMDAR antagonists (Cochran et al., 2003) and corresponding tissue loss. We confirmed tissue loss in the MK-PBO cohort with cresyl violet staining, revealing necrotic neurons and the appearance of Olney's lesions (Rothman and Olney, 1987). This sort of brain damage is typical after repeated administration of NMDAR antagonists in rodents, including PCP and MK801 (Horváth et al., 1997). Mechanisms that lead to hypometabolism possibly include spine disconnection and gradual retraction of the dendritic trees of pyramidal neurons in a protective response to potential excitotoxicity (Bustillo et al., 2012), thereby contributing to cell loss. Such is confirmed by the statistically significant correlation between tissue loss and decreased [^{18}F]-FDG uptake. The tissue preserving treatment effect of NAc is reflected in the attenuated metabolism reduction in the MK-NAc cohort at 2 weeks, though at 3 and 4 weeks this effect disappears transiently.

Microglial activation was monitored *in vivo* through static [^{18}F]-PBR111 scans and showed decreased uptake in the satellite MK-PBO cohort, while we did expect increased microglial activation and hence increased uptake. On the other hand OX42 immunostaining did show increased microglial activation after MK801 challenge in the satellite MK cohort, as was expected due to glutamate excitotoxicity causing brain damage and inflammation (Horváth

et al., 1997) (figure 1A(5-6)). In addition, also for the satellite MK-NAc cohort the results for the *in vivo* PET and *ex vivo* IHC are seemingly contradicting. Compared to the satellite MK-PBO cohort, the NAc treatment in the satellite MK-NAc cohort induced smaller decreases and even an increase in CG [^{18}F]-PBR111 uptake whereas the IHC staining revealed an anti-inflammatory effect through lower microglial activation score. We attribute our results partly to the tissue loss due to the NMDAR antagonism by MK801 causing glutamate excitotoxicity, as discussed in relation to the [^{18}F]-FDG results. We hypothesize that due to the tissue loss and consequently poor tissue perfusion, [^{18}F]-PBR111 scans could not detect the inflammatory increase that was demonstrated with immunostaining by a marker of microglial activation. Autoradiography confirmed that the tracer could indeed bind *in vitro* to activated microglia on the sections and could be specifically blocked by PK-11195 (data not shown). Slight tissue preservation by NAc is aided by direct scavenging of free radicals (Berk et al., 2013; Dean et al., 2012).

The microglial activation we demonstrated by IHC can be expected to contribute to increased levels of glutamate as well as neurotoxic TRYCAT pathway activation (Anderson and Maes, 2013). The conversion of TRP to KYN is the rate-limiting step of the TRYCAT pathway. The pathway preference can be assessed by the KYN to TRP ratio. This ratio is generally accepted to reflect IDO function. Indeed, this ratio increased significantly after two weeks only for the untreated MK-PBO cohort which most likely indicates pathway activation by MK801 and dampening by NAc for the treated MK-NAc group. Indeed, since NAc antagonises the function of IDO through depletion of superoxide anion radicals (needed as co-substrate for IDO), decreased formation of KYN is to be expected. The QA/KA ratio has been postulated to indicate NMDAR excitation and gives a sense of changes in the KA and QA (3-HK) arm of the TRYCAT pathway. Remarkedly, both this QA/KA ratio as well as the QA/KYN ratio is significantly increased for the Ctrl-NAc group at the end of the experiment. As the enzyme kynureninase down the QA arm of the pathway is highly vitamin B6 levels

dependent, NAc can stimulate the pathway towards QA production through protection of B6 against oxidation. Given that the KA/KYN ratio is signifcantly decreased after two weeks we hypothetize that there is a pathway shift towards the QA arm in the MK model which however accumulates at the 3-HK level through a vitamin B6 defiency in the presence of inflammation (Sakakeeny et al., 2012). Future experiments in this chronic MK-801 model need to also measure the 3-HK metabolite on HPLC to confirm.

Our results might indicate that in response to increased endogenous glutamate levels there is an upregulation of the TRYCAT pathway. Because of the clinical relevance, these findings should be translated to human studies. In general, the imbalance between the KA and 3HK arm in both directions might induce negative impact in terms of schizophrenia patients' positive symptoms development and impaired response to treatment (Myint et al., 2011). These type of studies are often useful as predictors and indicators of abnormal TRYCAT pathway function within the brain.

mGluR5 binding shows a subtle non significant increase in both PET and IHC data despite the aforementioned and proven major tissue loss. NAc was found not to counteract the effect of MK801 on mGluR5 binding, but in contrast further increased BP_{nd} and IOD values. Our findings indicate that chronic high glutamate levels induced by MK801 and/or NAc may upregulate mGluR5 binding. Several factors can contribute to this observation. Firstly, NAc itself can reduce the amplitude of glutamatergic activation in low concentrations. However, at higher concentrations, it has been shown that NAc can stimulate mGluR5-dependant glutamatergic synaptic currents, hereby reducing the therapeutic efficacy of NAc. (Kupchik et al., 2012). Secondly, NAc prevents excessive tissue damage, therefore there are more cells expressing the receptors. It should be noted however that mGluR5 availability measured with [^{11}C]-ABP688 PET has a complex relationship with mGluR5 binding of the neurons, in

that various factors could contribute to the decrease of its binding potential (Choi et al., 2014). In addition [^{11}C]-ABP688 measures reflect the mixture of primary pathology and compensatory changes of MK801 and NAc, adding to the complexity. Binding of [^{11}C]-ABP688 has shown to not be susceptible to acute changes in endogenous glutamate levels by MK801 and NAc in rats (Sandiego et al., 2013; Wyckhuys et al., 2013), therefore the binding of the ligand has been used in the current chronic setup to indicate receptor expression. Findings of the current study should be translated to clinical imaging studies. Thus far, genetic and postmortem studies continue to support the role of mGluR5 in schizophrenia pathology, yet do not conclusively show altered expression levels of the receptor (Newell and Matosin, 2014), or show decreased levels (Fatemi et al., 2013; Fatemi and Folsom, 2015). Molecular imaging provides the means to explore the regulation of mGLuR5 beyond total postmortem protein and mRNA levels.

Future research into therapeutic targets will be continued with respect to the role of mGluR5 and NMDAR, as well as acute studies to further elucidate binding properties of PET-tracers under endogenic glutamate fluctuations with for instance ketamine (DeLorenzo et al., 2014). Other variations of the NMDAR antagonism animal model with less excitotoxicity will be used for future research.

5. Conclusion

It has been shown that chronic MK801 administration causes neuronal damage and extensive tissue loss, hence hampering *in vivo* quantification techniques. A hyperactive pro-inflammatory response will upregulate the TRYCAT pathway in the activated microglia contributing again to increased glutamate via astrocytes. Chronic high glutamate levels may upregulate mGluR5 binding, which is of importance when targeting these receptors for development of antipsychotics. The obtained data stimulate further research on the interplay of neuro-inflammatory and glutamatergic pathways in the etiology of

schizophrenia.

Acknowledgements

We are grateful to prof. dr. Samir Kumar-Singh, Sofie Thys and dr. Isabel Pintelon of the laboratory of Cell Biology & Histology, UA for their support with the immunohistochemical studies, and to my colleague Philippe Joye of MICA, University of Antwerp for his help with the scan acquisitions.

Financial Disclosures

This work is supported by Antwerp University and its University Hospital through a technical position for Annemie Van Eetveldt and Robert Verkerk, a PhD fellowship for Lauren Kosten, a postdoctoral position for Leonie wyffels and Jeroen Verhaeghe, an assistant professorship for Stefanie Dedeurwaerdere, an associate professorship for Steven Staelens and a full professorship for Sigrid Stroobants. Livia De Picker is supported by IWT and David Thomae by FWO Pegasus. The project is in part funded by a UAntwerpen LP BOF grant and FWO grant G.0586.12. The authors declare to have no financial interests or potential conflicts of interest.

Figure captions

Figure 1: Illustration of the interplay between NMDAR, mGluR, energisation and microglia in relation the NMDA hypofunction hypothesis of schizophrenia with A) In glutamatergic neurons glutamine is converted through glutaminase into glutamate which is transported by VGLUT to be released in the synaptic cleft (1) where it post-synaptically binds (amongst others) to (i) mGluR5 to relay the excitatory signal to a connecting neuron, (ii) by mGluR2 as a negative feedback loop diminishing the glutamate release and (iii) by EAAT on neuroglia to terminate the excitatory signal converting glutamate back to glutamine via glutamine synthetase . This process is largely mediated by GABAergic neurons which take up glutamate through their NMDAR to release GABA in the synaptic cleft thereby inhibiting glutamatergic neurons (2). NMDAR antagonists such as MK801 cause a disinhibition by these GABAergic neurons with additional depletion of GSH due to oxidative stress (3). The energy source empowering excited neurons is mainly lactate which is anaerobically generated in astrocytes taking up glucose from the plasma via the glucose transporter 1 (GLUT1) and partly direct aerobic glycolysis in the neuron receiving plasma glucose via GLUT3 (4); Inflammation potentially influences these glutamatergic systems through glutamate release from microglia as an indirect consequence of GSH decrease and proinflammatory cytokines (5), and astrocyte stimulation by proinflammatory cytokines (6). This increases glutamate release and excessive astrocytic mGluR5 stimulation further amplifies the release of glutamate (7a) and neurotoxic ROS will also be released from dying neurons (7b). Recruited microglia then upregulate TSPO receptors upon activation (8). IC glutamate in astrocytes increases and expression of EAAT Glutamate transporters lowers during early stages of inflammation (9). N-Acetyl-cysteine (NAc) possibly exerts therapeutic effects, since it is known to indirectly increase extrasynaptic glutamate release through activation of the cystine–glutamate antiporter, hereby stimulating the mGluR2/3 and inhibiting glutamate release (10). NAc also has anti-inflammatory actions that dampen inflammation and improve

neuronal degeneration. As a glutathione precursor, NAc can increase GSH levels, which stimulates NMDAR activity, normalizing input to inhibitory GABA-ergic interneurons (11) and decreasing glutamate release from microglia (12). It can also effectively block CD11b expression, which is correlated to the severity of microglial activation (13). B) detail of the ionotropic NMDA receptor which is (i) ligand-gated requiring glutamate to bind with co-activation of D-serine or glycine and (ii) voltage-dependent through channel blocks by extracellular Zn2+ and Mg2+ ions; C) detail of the metabotropic mGluR5 receptor which is a G-protein coupled receptor with the N-terminal extracellular for binding a ligand through the venus fly trap mechanism causing a conformational change activating the G-protein of which the alpha subunit causes a downstream cascade and with allosteric binding sites in the 7 transmembrane domain receptors. D) The kynurenine (TRYCAT) pathway is a major catabolic cascade of tryptophan (TRP) that is activated in microglia by pro-inflammatory cytokines. It splits in two arms, one producing neurotoxic 3-HK and QA the other producing the endogenous neuroprotective NMDAR antagonist KA.

Figure 2: Overview of experimental cohorts, longitudinal scans and protocols. A) Challenge, treatment and evaluations for each cohort. Ex vivo IHC occurred end of life. Plasma samples for TRYCAT metabolite analyses were taken at 3 timepoints. B) protocol of the [^{18}F]-FDG scans for neuronal metabolism. C) protocol of the [^{18}F]-PBR111 scans for microglial activation. D) protocol of the [^{11}C]-ABP688 dynamic scans for mGluR5.

Figure 3: Percentage (mean ± SEM) change in [^{18}F]-FDG uptake SUV compared to baseline. A) Caudate putamen. B) Medial prefrontal cortex. C) Cingulate cortex. D) Hippocampus. Expressed are means ± SEM. [^{18}F]-PBR111 ratio of brain activity over plasma activity 30 min p.i. (kBq/cc), percentage change to baseline. E) Caudate putamen. F) Medial prefrontal cortex. G) Cingulate cortex. H) Hippocampus. Expressed as means ± SEM. [^{11}C]-ABP688

BP_{nd}. I) Caudate Putamen. J) Medial Prefrontal Cortex. K) Cingulate cortex. L) Hippocampus. Expressed are means ± SEM * $p<0.05$

Figure 4: (A) Cresyl violet IHC showing tissue damage at t=4w expressed in % damaged tissue as means ± SEM from at least five different 40x images per brain region. (B) OX42 mean scores ± SEM of microglia at t=4w for the control and schizophrenia–like cohort. The score reflects the OX42-stained cell number, activation and intensity in at least five different 40x images per brain region of the most densely stained areas. C) Intrinsic Optical density (mean ± SEM) of the mGluR5 IHC. * $p<0.05$

Figure 5: HPLC analysis for plasma metabolites: concentration ratio. A) Kynurenine/tryptophan. B) Kynurenic acid/Kynurenine. C) Quinolinic Acid/kynurenine. D) Quinolinic Acid/Kynurenic Acid. Expressed are mean ± SEM. * $p<0.05$, ** $p<0.01$, *** $p<0.001$

References

Adams, R., David, A.S., 2007. Patterns of anterior cingulate activation in schizophrenia: a selective review. Neuropsychiatr Dis Treat 3, 87–101.

Adams, R.A., Stephan, K.E., Brown, H.R., Frith, C.D., Friston, K.J., 2013. The computational anatomy of psychosis. Front Psychiatry 4, 47. doi:10.3389/fpsyt.2013.00047

Anderson, G., Maes, M., 2013. Schizophrenia: linking prenatal infection to cytokines, the tryptophan catabolite (TRYCAT) pathway, NMDA receptor hypofunction, neurodevelopment and neuroprogression. Prog. Neuropsychopharmacol. Biol. Psychiatry 42, 5–19. doi:10.1016/j.pnpbp.2012.06.014

Anderson, G., Maes, M., Berk, M., 2013. Schizophrenia is primed for an increased expression of depression through activation of immuno-inflammatory, oxidative and nitrosative stress, and tryptophan catabolite pathways. Prog. Neuropsychopharmacol. Biol. Psychiatry 42, 101–114. doi:10.1016/j.pnpbp.2012.07.016

Barger, S.W., Goodwin, M.E., Porter, M.M., Beggs, M.L., 2007. Glutamate release from activated microglia requires the oxidative burst and lipid peroxidation. Journal of Neurochemistry 101, 1205–1213. doi:10.1111/j.1471-4159.2007.04487.x

Bayer, T.A., Buslei, R., Havas, L., Falkai, P., 1999. Evidence for activation of microglia in patients with psychiatric illnesses. Neurosci. Lett.

Berk, M., Malhi, G.S., Gray, L.J., Dean, O.M., 2013. The promise of N-acetylcysteine in neuropsychiatry. Trends Pharmacol. Sci. 34, 167–177. doi:10.1016/j.tips.2013.01.001

Bubeníková-Valešová, V., Horáček, J., Vrajová, M., Höschl, C., 2008. Models of schizophrenia in humans and animals based on inhibition of NMDA receptors. Neuroscience & Biobehavioral Reviews 32, 1014–1023. doi:10.1016/j.neubiorev.2008.03.012

Bustillo, J., Galloway, M.P., Ghoddoussi, F., Bolognani, F., Perrone-Bizzozero, N., 2012. Medial-frontal cortex hypometabolism in chronic phencyclidine exposed rats assessed by high resolution magic angle spin 11.7 T proton magnetic resonance spectroscopy. Neurochemistry International 61, 128–131. doi:10.1016/j.neuint.2012.04.003

Chen, Y., Guillemin, G.J., 2009. Kynurenine pathway metabolites in humans: disease and healthy States. Int J Tryptophan Res 2, 1–19.

Choi, H., Kim, Y.K., Oh, S.W., Im, H.-J., Hwang, D.W., Kang, H., Lee, B., Lee, Y.-S., Jeong, J.M., Kim, E.E., Chung, J.-K., Lee, D.S., 2014. In vivo imaging of mGluR5 changes during epileptogenesis using [11C]ABP688 PET in pilocarpine-induced epilepsy rat model. PLoS ONE 9, e92765. doi:10.1371/journal.pone.0092765

Cochran, S.M., Kennedy, M., McKerchar, C.E., Steward, L.J., Pratt, J.A., Morris, B.J., 2003. Induction of metabolic hypofunction and neurochemical deficits after chronic intermittent exposure to phencyclidine: differential modulation by antipsychotic drugs. Neuropsychopharmacology 28, 265–275. doi:10.1038/sj.npp.1300031

Dean, O.M., Bush, A.I., Berk, M., 2012. Translating the Rosetta Stone of N-Acetylcysteine. Biol. Psychiatry 71, 935–936. doi:10.1016/j.biopsych.2012.04.001

Deleye, S., Verhaeghe, J., Wyffels, L., Dedeurwaerdere, S., Stroobants, S., Staelens, S., 2014. Towards a reproducible protocol for repetitive and semi-quantitative rat brain imaging with (18) F-FDG: Exemplified in a memantine pharmacological challenge. NeuroImage 96C, 276–287. doi:10.1016/j.neuroimage.2014.04.004

DeLorenzo, C., DellaGioia, N., bloch, M., Sanacora, G., Nabulsi, N., Abdallah, C., Yang, J., Wen, R., Mann, J.J., Krystal, J.H., Parsey, R.V., Carson, R.E., Esterlis, I., 2014. In Vivo Ketamine-Induced Changes in [(11)C]ABP688 Binding to Metabotropic Glutamate Receptor Subtype 5. Biol. Psychiatry. doi:10.1016/j.biopsych.2014.06.024

Deschwanden, A., Karolewicz, B., Feyissa, A.M., Treyer, V., Ametamey, S.M., Johayem, A., Burger, C., Auberson, Y.P., Sovago, J., Stockmeier, C.A., Buck, A., Hasler, G., 2011. Reduced metabotropic glutamate receptor 5 density in major depression determined by [(11)C]ABP688 PET and postmortem study. Am J Psychiatry 168, 727–734. doi:10.1176/appi.ajp.2011.09111607

Elmenhorst, D., Aliaga, A., Bauer, A., Rosa-Neto, P., 2012. Test-retest stability of cerebral $mGluR_5$ quantification using [^{11}C]ABP688 and positron emission tomography in rats. Synapse 66, 552–560. doi:10.1002/syn.21542

Eyjolfsson, E.M., Brenner, E., Kondziella, D., Sonnewald, U., 2006. Repeated injection of MK801: An animal model of schizophrenia? Neurochemistry International 48, 541–546. doi:10.1016/j.neuint.2005.11.019

Fatemi, S.H., Folsom, T.D., 2015. GABA receptor subunit distribution and FMRP-mGluR5 signaling abnormalities in the cerebellum of subjects with schizophrenia, mood disorders, and autism. Schizophr. Res. 167, 42–56. doi:10.1016/j.schres.2014.10.010

Fatemi, S.H., Folsom, T.D., Rooney, R.J., Thuras, P.D., 2013. mRNA and protein expression for novel GABAA receptors θ and ρ2 are altered in schizophrenia and mood disorders; relevance to FMRP-mGluR5 signaling pathway. Transl Psychiatry 3, e271. doi:10.1038/tp.2013.46

Fookes, C.J.R., Pham, T.Q., Mattner, F., Greguric, I., Loc'h, C., Liu, X., Berghofer, P., Shepherd, R., Grégoire, M.-C., Katsifis, A., 2008. Synthesis and Biological Evaluation of Substituted [18F]Imidazo[1,2- a]pyridines and [18F]Pyrazolo[1,5- a]pyrimidines for the Study of the Peripheral Benzodiazepine Receptor Using Positron Emission Tomography. J. Med. Chem. 51, 3700–3712. doi:10.1021/jm7014556

Frick, L.R., Williams, K., Pittenger, C., 2013. Microglial dysregulation in psychiatric disease. Clin. Dev. Immunol. 2013, 608654. doi:10.1155/2013/608654

Gaspar, P.A., Bustamante, M.L., Silva, H., Aboitiz, F., 2009. Molecular mechanisms underlying glutamatergic dysfunction in schizophrenia: therapeutic implications. Journal of Neurochemistry 111, 891–900. doi:10.1111/j.1471-4159.2009.06325.x

Hashimoto, K., Malchow, B., Falkai, P., Schmitt, A., 2013. Glutamate modulators as potential therapeutic drugs in schizophrenia and affective disorders. Eur Arch Psychiatry Clin Neurosc 263, 367–377. doi:10.1007/s00406-013-0399-y

Horváth, Z.C., Czopf, J., Buzsáki, G., 1997. MK-801-induced neuronal damage in rats. Brain Research 753, 181–195. doi:10.1016/S0006-8993(96)01290-5

Huang, Y.-R., Shih, J.-M., Chang, K.-W., Huang, C., Wu, Y.-L., Chen, C.-C., 2012. [123I]Epidepride neuroimaging of dopamine D2/D3 receptor in chronic MK-801-induced rat schizophrenia model. Nucl. Med. Biol. 39, 826–832. doi:10.1016/j.nucmedbio.2012.01.005

Kupchik, Y.M., Moussawi, K., Tang, X.-C., Wang, X., Kalivas, B.C., Kolokithas, R., Ogburn, K.B., Kalivas, P.W., 2012. The effect of N-acetylcysteine in the nucleus accumbens on neurotransmission and relapse to cocaine. Biol. Psychiatry 71, 978–986. doi:10.1016/j.biopsych.2011.10.024

Matosin, N., Newell, K.A., 2013. Metabotropic glutamate receptor 5 in the pathology and treatment of schizophrenia. Neuroscience & Biobehavioral Reviews 37, 256–268. doi:10.1016/j.neubiorev.2012.12.005

Meador-Woodruff, J., 2000. Glutamate receptor expression in schizophrenic brain. Brain Research Reviews 31, 288–294. doi:10.1016/S0165-0173(99)00044-2

Miyake, N., Skinbjerg, M., Easwaramoorthy, B., Kumar, D., Girgis, R.R., Xu, X., Slifstein, M., Abi-Dargham, A., 2011. Imaging changes in glutamate transmission in vivo with the metabotropic glutamate receptor 5 tracer [11C] ABP688 and N-acetylcysteine challenge.

Biol. Psychiatry 69, 822–824. doi:10.1016/j.biopsych.2010.12.023
Myint, A.M., 2012. Kynurenines: from the perspective of major psychiatric disorders. FEBS J. 279, 1375–1385. doi:10.1111/j.1742-4658.2012.08551.x
Myint, A.M., Schwarz, M.J., Verkerk, R., Mueller, H.H., Zach, J., Scharpé, S., Steinbusch, H.W.M., Leonard, B.E., Kim, Y.K., 2011. Reversal of imbalance between kynurenic acid and 3-hydroxykynurenine by antipsychotics in medication-naïve and medication-free schizophrenic patients. Brain Behav. Immun. 25, 1576–1581. doi:10.1016/j.bbi.2011.05.005
Nakazawa, K., Zsiros, V., Jiang, Z., Nakao, K., Kolata, S., Zhang, S., Belforte, J.E., 2012. GABAergic interneuron origin of schizophrenia pathophysiology. Neuropharmacology 62, 1574–1583. doi:10.1016/j.neuropharm.2011.01.022
Newell, K.A., Matosin, N., 2014. Rethinking metabotropic glutamate receptor 5 pathological findings in psychiatric disorders: implications for the future of novel therapeutics. BMC Psychiatry 14, 23. doi:10.1186/1471-244X-14-23
Park, H.-J., Lee, J.D., Chun, J.W., Seok, J.H., Yun, M., Oh, M.-K., Kim, J.-J., 2006. Cortical surface-based analysis of 18F-FDG PET: Measured metabolic abnormalities in schizophrenia are affected by cortical structural abnormalities. NeuroImage 31, 1434–1444. doi:10.1016/j.neuroimage.2006.02.001
Poels, E.M.P., Kegeles, L.S., Kantrowitz, J.T., Slifstein, M., Javitt, D.C., Lieberman, J.A., Abi-Dargham, A., Girgis, R.R., 2014. Imaging glutamate in schizophrenia: review of findings and implications for drug discovery. Mol. Psychiatry 19, 20–29. doi:10.1038/mp.2013.136
Preti, A., Wilson, D.R., 2011. Schizophrenia, Cancer and Obstetric Complications in an Evolutionary Perspective-An Empirically Based Hypothesis. Psychiatry Investigation 8, 77–88. doi:10.4306/pi.2011.8.2.77
Radonjić, N.V., Knežević, I.D., Vilimanovich, U., Kravić-Stevović, T., Marina, L.V., Nikolić, T., Todorović, V., Bumbaširević, V., Petronijević, N.D., 2010. Decreased glutathione levels and altered antioxidant defense in an animal model of schizophrenia: Long-term effects of perinatal phencyclidine administration. Neuropharmacology 58, 739–745. doi:10.1016/j.neuropharm.2009.12.009
Rothman, S.M., Olney, J.W., 1987. Excitotoxity and the NMDA receptor. Trends in Neurosciences 10, 299–302. doi:10.1016/0166-2236(87)90177-9
Sakakeeny, L., Roubenoff, R., Obin, M., Fontes, J.D., Benjamin, E.J., Bujanover, Y., Jacques, P.F., Selhub, J., 2012. Plasma Pyridoxal-5-Phosphate Is Inversely Associated with Systemic Markers of Inflammation in a Population of U.S. Adults. Journal of Nutrition 142, 1280–1285. doi:10.3945/jn.111.153056
Sandiego, C.M., Nabulsi, N., Lin, S.-F., Labaree, D., Najafzadeh, S., Huang, Y., Cosgrove, K., Carson, R.E., 2013. Studies of the metabotropic glutamate receptor 5 radioligand [^{11}C]ABP688 with N-acetylcysteine challenge in rhesus monkeys. Synapse 67, 489–501. doi:10.1002/syn.21656
Sorg, C., Manoliu, A., Neufang, S., Myers, N., Peters, H., Schwerthöffer, D., Scherr, M., Mühlau, M., Zimmer, C., Drzezga, A., Förstl, H., Bäuml, J., Eichele, T., Wohlschläger, A.M., Riedl, V., 2013. Increased intrinsic brain activity in the striatum reflects symptom dimensions in schizophrenia. Schizophrenia Bulletin 39, 387–395. doi:10.1093/schbul/sbr184
Soyka, M., Koch, W., Möller, H.J., Rüther, T., Tatsch, K., 2005. Hypermetabolic pattern in frontal cortex and other brain regions in unmedicated schizophrenia patients. Eur Arch Psychiatry Clin Neurosc 255, 308–312. doi:10.1007/s00406-005-0563-0
Tsukada, H., Nishiyama, S., Fukumoto, D., Kanazawa, M., Harada, N., 2014. Novel PET probes 18F-BCPP-EF and 18F-BCPP-BF for mitochondrial complex I: a PET study in comparison with 18F-BMS-747158-02 in rat brain. J. Nucl. Med. 55, 473–480.

doi:10.2967/jnumed.113.125328
van Berckel, B.N., Bossong, M.G., Boellaard, R., Kloet, R., Schuitemaker, A., Caspers, E., Luurtsema, G., Windhorst, A.D., Cahn, W., Lammertsma, A.A., Kahn, R.S., 2008. Microglia Activation in Recent-Onset Schizophrenia: A Quantitative (R)-[11C]PK11195 Positron Emission Tomography Study. Biol. Psychiatry 64, 820–822. doi:10.1016/j.biopsych.2008.04.025
Van den Eynde, K., Missault, S., Fransen, E., Raeymaekers, L., Willems, R., Drinkenburg, W., Timmermans, J.-P., Kumar-Singh, S., Dedeurwaerdere, S., 2014. Hypolocomotive behaviour associated with increased microglia in a prenatal immune activation model with relevance to schizophrenia. Behav. Brain Res. 258, 179–186. doi:10.1016/j.bbr.2013.10.005
van Os, J., Kapur, S., 2009. Schizophrenia. Lancet 374, 635–645. doi:10.1016/S0140-6736(09)60995-8
Vinson, P.N., Conn, P.J., 2012. Metabotropic glutamate receptors as therapeutic targets for schizophrenia. Neuropharmacology 62, 1461–1472. doi:10.1016/j.neuropharm.2011.05.005
Wang, B., Navath, R.S., Romero, R., Kannan, S., Kannan, R., 2009. Anti-inflammatory and anti-oxidant activity of anionic dendrimer–N-acetyl cysteine conjugates in activated microglial cells. International Journal of Pharmaceutics 377, 159–168. doi:10.1016/j.ijpharm.2009.04.050
Whitfield-Gabrieli, S., Thermenos, H.W., Milanovic, S., Tsuang, M.T., Faraone, S.V., McCarley, R.W., Shenton, M.E., Green, A.I., Nieto-Castanon, A., LaViolette, P., Wojcik, J., Gabrieli, J.D.E., Seidman, L.J., 2009. Hyperactivity and hyperconnectivity of the default network in schizophrenia and in first-degree relatives of persons with schizophrenia. Proc. Natl. Acad. Sci. U.S.A. 106, 1279–1284. doi:10.1073/pnas.0809141106
Wyckhuys, T., Verhaeghe, J., Wyffels, L., Langlois, X., Schmidt, M., Stroobants, S., Staelens, S., 2013. N-Acetylcysteine- and MK-801-Induced Changes in Glutamate Levels Do Not Affect In Vivo Binding of Metabotropic Glutamate 5 Receptor Radioligand 11C-ABP688 in Rat Brain. J. Nucl. Med. doi:10.2967/jnumed.113.121608
Wyckhuys, T., Wyffels, L., Langlois, X., Schmidt, M., Stroobants, S., Staelens, S., 2014. The [18F]FDG μPET readout of a brain activation model to evaluate the metabotropic glutamate receptor 2 positive allosteric modulator JNJ-42153605. J. Pharmacol. Exp. Ther. 350, 375–386. doi:10.1124/jpet.114.213959
Zantomio, D., Chana, G., Laskaris, L., Testa, R., Everall, I., Pantelis, C., Skafidas, E., 2015. Convergent evidence for mGluR5 in synaptic and neuroinflammatory pathways implicated in ASD. Neuroscience & Biobehavioral Reviews 52, 172–177. doi:10.1016/j.neubiorev.2015.02.006

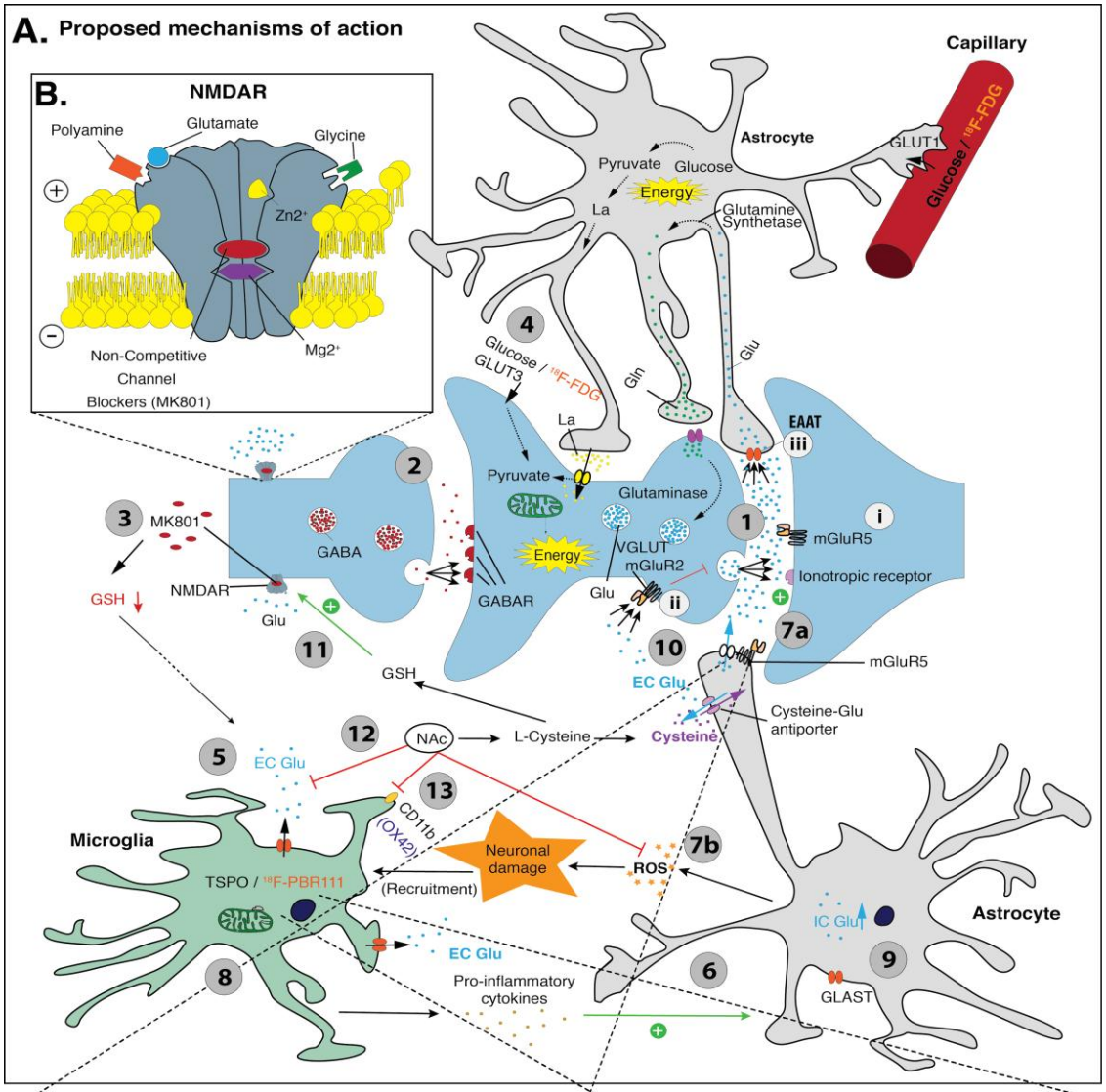
A. Proposed mechanisms of action
B. NMDAR
Polyamine
Glutamate
Glycine
Zn2+
Mg2+
Non-Competitive Channel Blockers (MK801)
Capillary
Astrocyte
GLUT1
Glucose / 18F-FDG
Pyruvate
Glucose
Energy
La
Glutamine Synthetase
Glu
Gln
GLUT3
EAAT
iii
i
mGluR5
Ionotropic receptor
ii
mGluR2
VGLUT
Glutaminase
Pyruvate
La
Energy
GABA
GABAR
MK801
NMDAR
GSH
Glu
EC Glu
Cysteine-Glu antiporter
Cysteine
NAc
L-Cysteine
CD11b (OX42)
(Recruitment)
Neuronal damage
ROS
Microglia
TSPO / 18F-PBR111
IC Glu
GLAST
Pro-inflammatory cytokines
C. mGluR5
N-terminal extracellular ligand-binding domain
7-TM domain
Intracellular C-terminal domain
Competitive agonists / antagonists (Glu)
Non-Competitive antagonists (11C-ABP688)
PKA
ATP
cAMP
Adenylyl Cyclase
GTP
GDP
D. TRYCAT
anti-inflammatory
pro-inflammatory
IL-4
IFN-Y
Tryptophan
5-HT
IDO
TDO
Kynurenine
KAT
3-HK
KA
Kynureninase
3-OH Anth
QA
Legend
GABA gamma-aminobutyric acid
Glu glutamate
Gln glutamine
La lactate
MK801 dizocilpine
ROS Reactive oxygen species
Cysteine
Cytokines
ATP Adenosine triphosphate
cAMP Cyclic adenosine monophosphate
EAAT excitatory amino acid transporter
EC Extracellular
GDP Guanosine diphosphate
GLAST Glutamate transporter
GLUT glucose transporter
GTP Guanosine triphosphate
GSH Glutathione
IC Intracellular
IFN Interferon
IL Interleukin
KA Kynurenic acid
mGluR metabotropic glutamate receptor
NAc N-Acteyl-cysteine
NMDAR N-methyl-D-aspartate receptor
PKA Protein Kinase A
QA Quinolinic acid

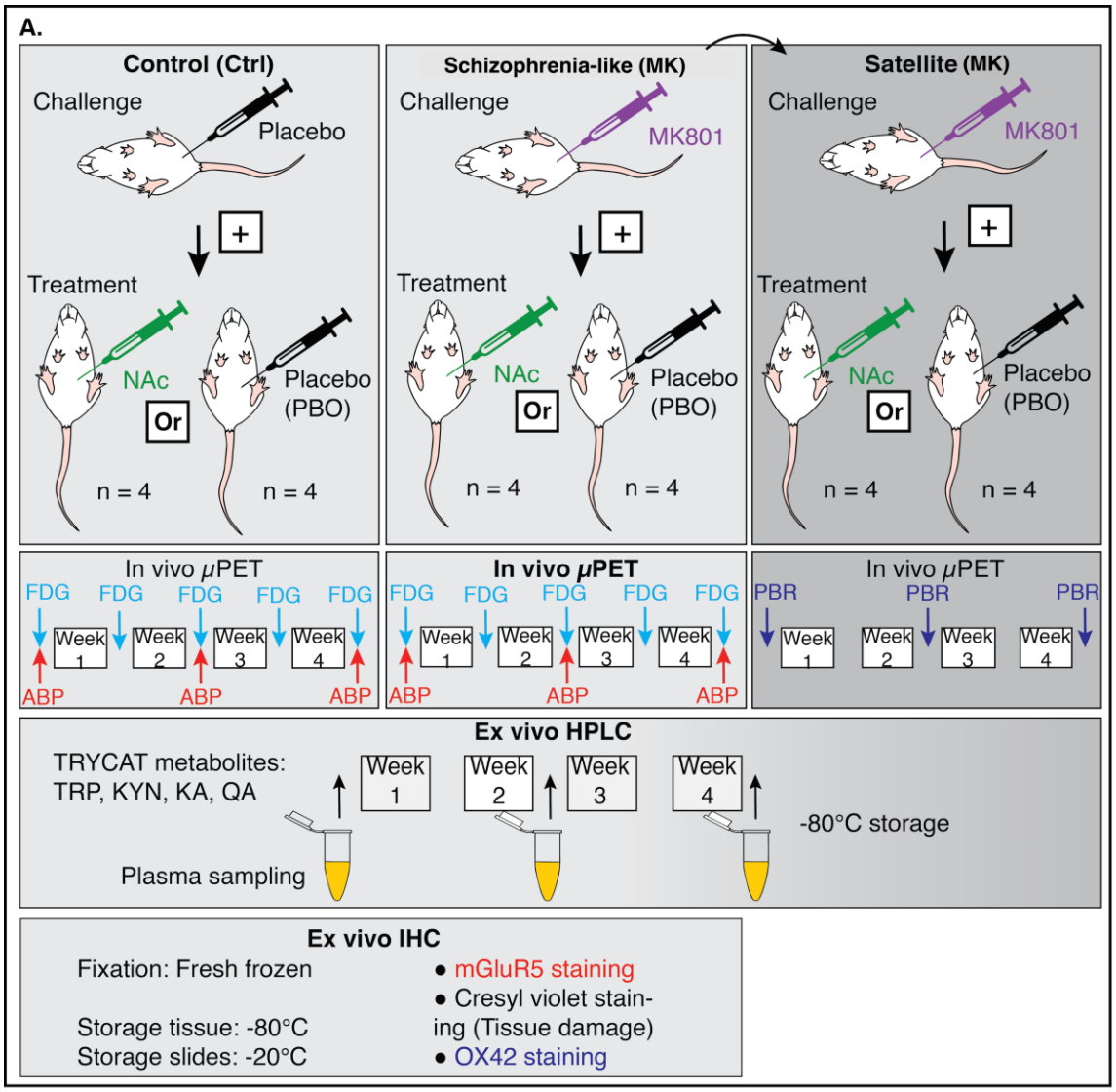
A.
Control (Ctrl)
Challenge
Placebo
+
Treatment
NAc
Or
Placebo (PBO)
n = 4
n = 4
Schizophrenia-like (MK)
Challenge
MK801
+
Treatment
NAc
Or
Placebo (PBO)
n = 4
n = 4
Satellite (MK)
Challenge
MK801
+
Treatment
NAc
Or
Placebo (PBO)
n = 4
n = 4
In vivo μPET
FDG FDG FDG FDG FDG
Week 1 Week 2 Week 3 Week 4
ABP ABP ABP
In vivo μPET
FDG FDG FDG FDG FDG
Week 1 Week 2 Week 3 Week 4
ABP ABP ABP
In vivo μPET
PBR PBR PBR
Week 1 Week 2 Week 3 Week 4
Ex vivo HPLC
TRYCAT metabolites:
TRP, KYN, KA, QA
Week 1 Week 2 Week 3 Week 4
Plasma sampling
-80°C storage
Ex vivo IHC
Fixation: Fresh frozen
Storage tissue: -80°C
Storage slides: -20°C
• mGluR5 staining
• Cresyl violet staining (Tissue damage)
• OX42 staining

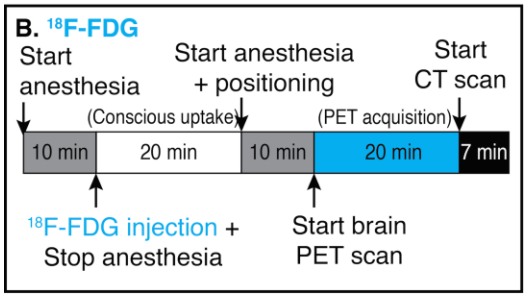
B. 18F-FDG
Start anesthesia
Start anesthesia + positioning
Start CT scan
(Conscious uptake)
(PET acquisition)
10 min
20 min
10 min
20 min
7 min
18F-FDG injection + Stop anesthesia
Start brain PET scan

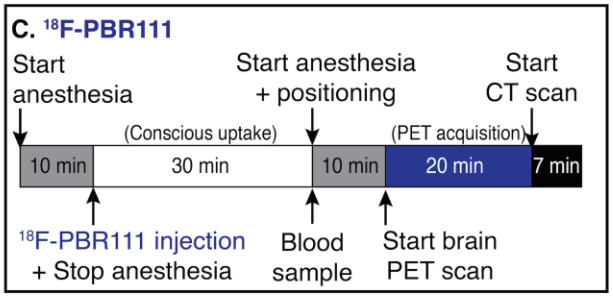
C. 18F-PBR111
Start anesthesia
Start anesthesia + positioning
Start CT scan
(Conscious uptake)
(PET acquisition)
10 min
30 min
10 min
20 min
7 min
18F-PBR111 injection + Stop anesthesia
Blood sample
Start brain PET scan

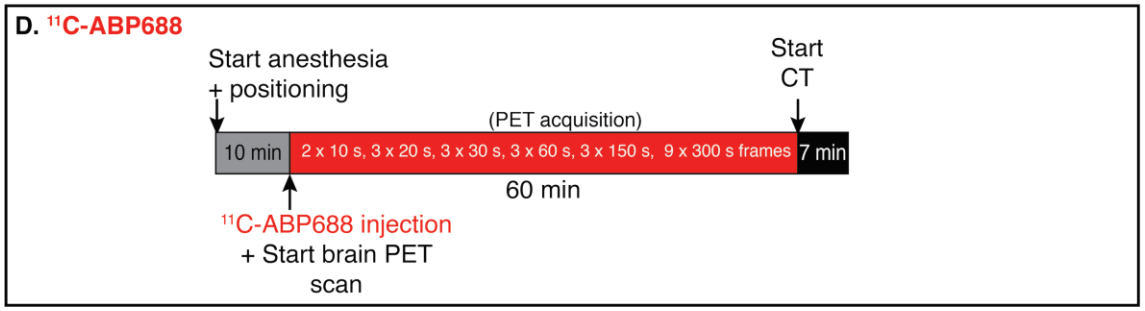
D. 11C-ABP688
Start anesthesia + positioning
Start CT
(PET acquisition)
10 min
2 x 10 s, 3 x 20 s, 3 x 30 s, 3 x 60 s, 3 x 150 s, 9 x 300 s frames
7 min
60 min
11C-ABP688 injection + Start brain PET scan

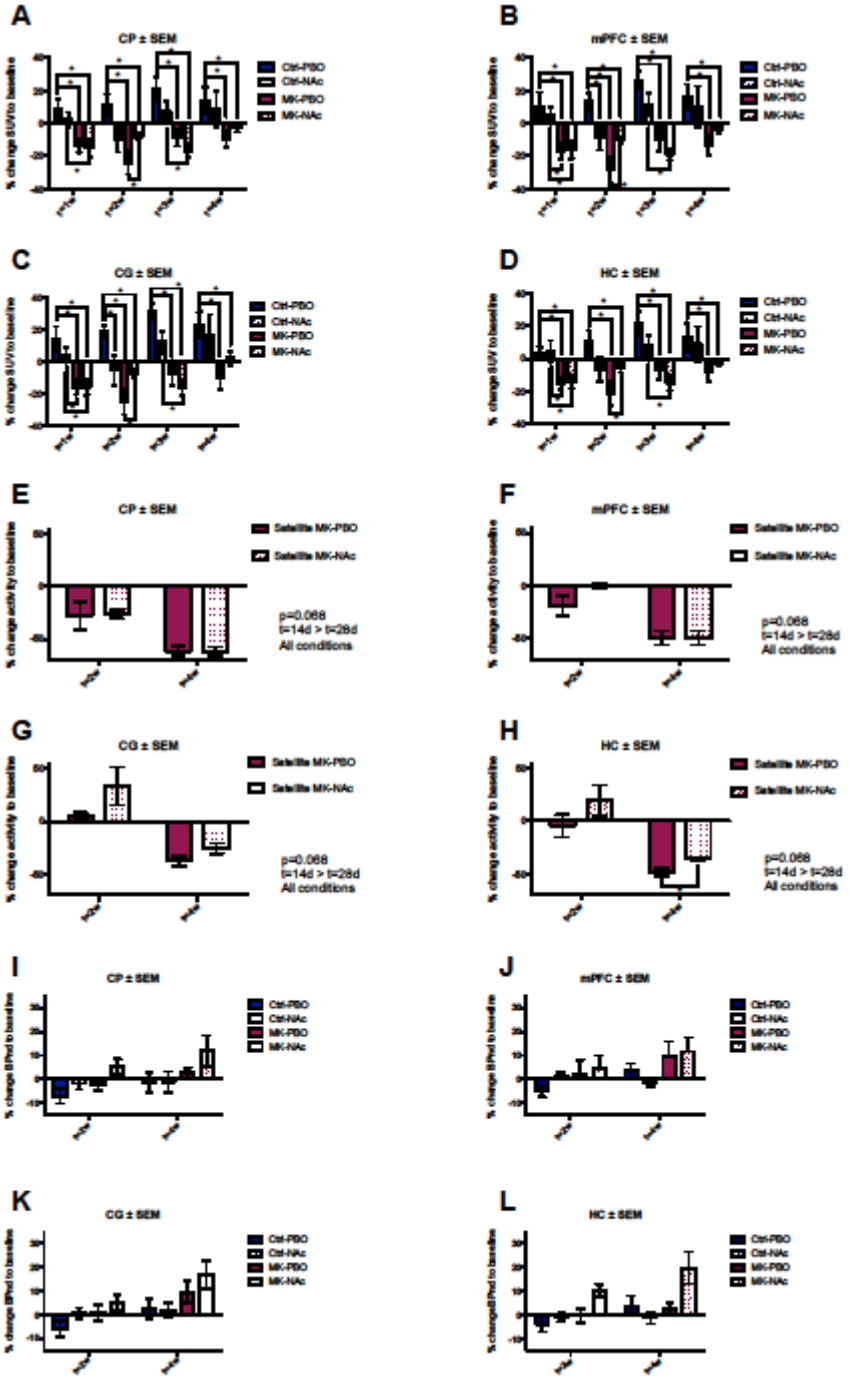
A
CP ± SEM
B
mPFC ± SEM
C
CG ± SEM
D
HC ± SEM
Ctrl-PBO
Ctrl-NAc
MK-PBO
MK-NAc
E
CP ± SEM
F
mPFC ± SEM
G
CG ± SEM
H
HC ± SEM
Satellite MK-PBO
Satellite MK-NAc
p=0.068
t=14d > t=28d
All conditions
I
CP ± SEM
J
mPFC ± SEM
K
CG ± SEM
L
HC ± SEM

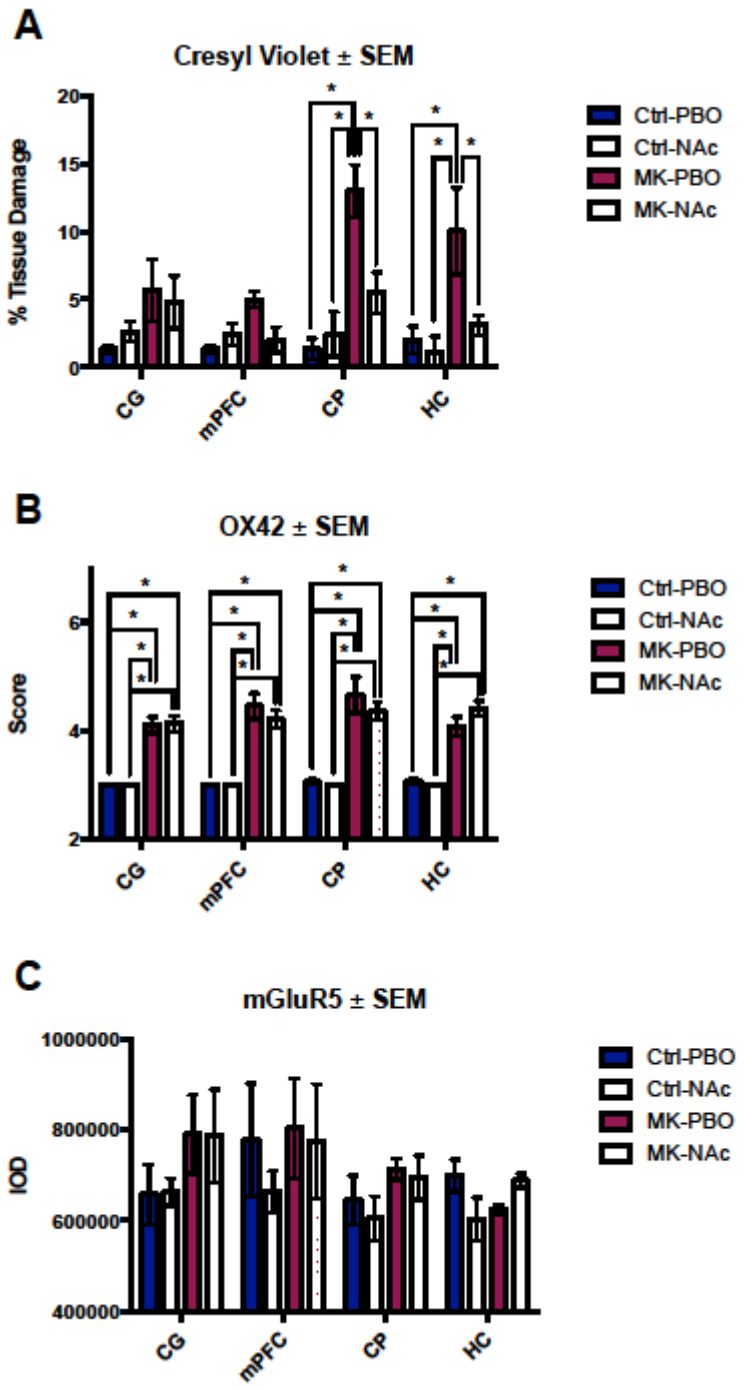
A
Cresyl Violet ± SEM
% Tissue Damage
20
15
10
5
0
CG
mPFC
CP
HC
Ctrl-PBO
Ctrl-NAc
MK-PBO
MK-NAc
B
OX42 ± SEM
Score
6
4
2
CG
mPFC
CP
HC
Ctrl-PBO
Ctrl-NAc
MK-PBO
MK-NAc
C
mGluR5 ± SEM
IOD
1000000
800000
600000
400000
CG
mPFC
CP
HC
Ctrl-PBO
Ctrl-NAc
MK-PBO
MK-NAc

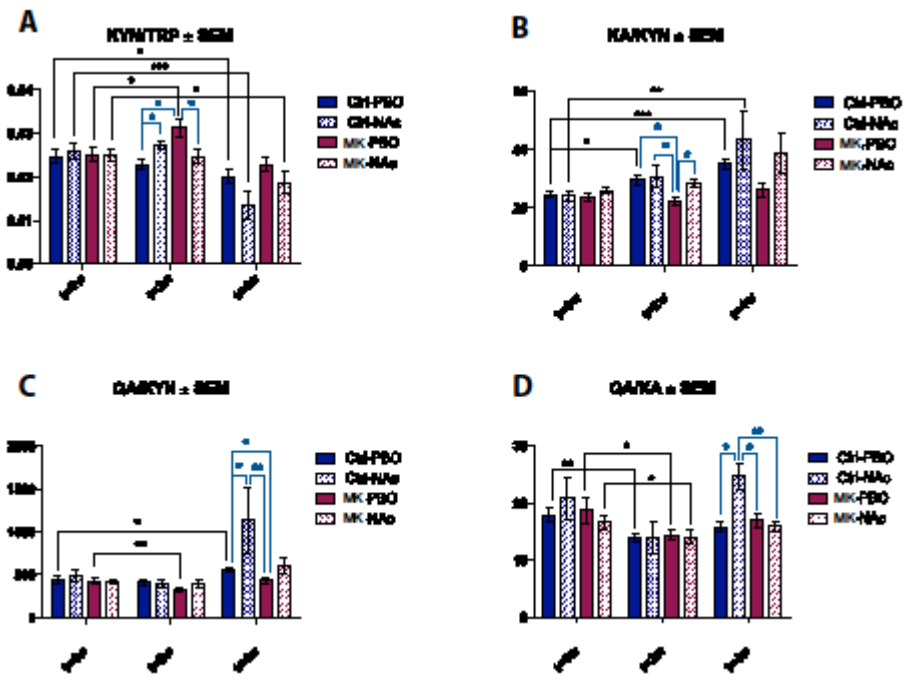

Highlights

- The first longitudinal multiprobe μPET study in a NMDAR hypofunction rat model;
- Chronic high glutamate tends to upregulate mGluR5 expression or shift the affinity;
- Microglial activation appears to amplify already increased glutamate levels;
- TRYCAT pathway overactivation contributes to the pathology;

- Targeting mGluR5 receptors for antipsychotics development remains promising.